International Journal of Mechanical Sciences 205 (2021) 106605

Contents lists available at ScienceDirect

International Journal of Mechanical Sciences

journal homepage: www.elsevier.com/locate/ijmecsci

Analysis of stability and stick-slip motion of a friction-induced vibrating system with dwell-time effect

N.N. Hieu [a,b,c,*], P.N. Chung [d]

[a] Faculty of Mechanical Engineering and Mechatronics, Phenikaa University, To Huu Str., Yen Nghia Ward, Ha Dong Dist., Hanoi, Vietnam
[b] Phenikaa Research and Technology Institute (PRATI), A&A Green Phoenix Group SJC, 167 Hoang Ngan Str., Trung Hoa Ward, Cau Giay Dist., Hanoi, Vietnam
[c] Institute of Mechanics, Vietnam Academy of Science and Technology, 264 Doi Can Str., Ba Dinh, Hanoi, Vietnam
[d] Faculty of Basic Science, University of Mining and Geology, 18 Vien Str., Duc Thang Ward, Bac Tu Liem Dist., Hanoi, Vietnam

ARTICLE INFO

Keywords:
Stick-slip
Dwell-time
Low-velocity
Stability
Limit cycle

ABSTRACT

In this paper, the authors investigate the stability and stick-slip motion of a friction-induced vibrating system placed on a belt moving at constant velocity using two-state model with consideration of dwell-time effect. The two-state model can be considered as an extension of the LuGre model because it can capture both Stribeck and dwell-time effects in the case of near-zero relative motion velocity between two surfaces. The previously known Stribeck effect is that the friction force decreases as the relative velocity increases in the near-zero range, while the dwell-time effect exhibits that the friction force increases as two surfaces are kept in contact for a certain time. With new effect of dwell-time, properties of stick-slip motion are explored in detail, including the equilibrium point position, the stability of the equilibrium point, Hopf bifurcation, characteristics of velocity and the change of friction force in different cases of belt velocity. The obtained result indicates that the influence of dwell-time on system responses is significant in the near-zero velocity range. Using the Routh-Hurwitz criterion, the authors show that there is a positive shift in the direction of increase of belt velocity for the stable zone of the equilibrium position compared with the stable zone obtained from the LuGre model. The formulations of the limit cycle and phases of motion in stick-slip vibration of the system are demonstrated by numerical simulations.

1. Introduction

In engineering systems, the friction exhibits diverse behaviors, especially when it comes from friction-induced vibrations [1–6]. Stick-slip phenomena in friction-induced vibrating systems can be observed in real systems, for example, the sound of bowed instrument, rattling joints of a robot, chattering machine tools [7–10], drill string systems [11], aircraft brake system [12]. In [8], Oetstreich investigated the bifurcation and stability for models of non-smooth friction oscillators with stick-slip motion using the mapping approach that gives insight into the periodic as well as the chaotic behavior of the system. In a research by Pratt and Williams [9], nonlinear analysis of stick-slip motion of a two-mass system with dry (Coulomb) friction contact was performed using a combined analytical-numerical procedure. In [10], approximate analytical expressions utilizing the method of perturbation are derived for the conditions, amplitudes, and base frequencies of stick-slip and pure-slip oscillations. Another interesting engineering system that exhibits stick-slip motion is drill string system [11]. Stick-slip oscillations due to the contact between the drilling bit and formation is known to excite severe torsional and axial vibrations in the drill string system. Vibrational characteristics of rotating drill string are investigated by a finite element dynamic formulation. In a detailed research by Sinou et al. [12], a non-linear model for friction-induced vibration analysis of aircraft brake whirl is presented and developed based on experimental observations. Those authors have shown that there is a perfect correlation between the numerical model and experimental tests for frequency of instability and deformation shape of the unstable mode.

In most engineering systems, to explore characteristics of vibrating systems that account for the friction effect, two kinds of friction behavior are used, namely, the static and dynamic friction [13–15]. Static friction is friction between two or more solid objects that are not moving relative to each other. Dynamic friction occurs when two objects are moving relative to each other and rub together. The static friction models are those that can be expressed as functions of relative velocity between two surfaces in contact. For static models, the Coulomb [16] and viscous friction models [17,18] are two simple models often used in theoretical and experimental studies in the field of tribology. In the Coulomb model, the friction force is constant and opposite to the direction of motion. In the viscous model, the friction force is proportional to the velocity. These models only describe the steady-state behavior between velocity and friction force. They are suitable for case

* Corresponding author.
E-mail addresses: hieu.nguyennhu@phenikaa-uni.edu.vn (N.N. Hieu), phamngocchung@humg.edu.vn (P.N. Chung).

https://doi.org/10.1016/j.ijmecsci.2021.106605
Received 24 September 2020; Received in revised form 27 May 2021; Accepted 15 June 2021
Available online 23 June 2021

of enough large velocity of system motion. In the range of low velocity, one may look for an appropriate model to describe real systems in a more precise manner. Models of dynamic friction are candidates to capture different effects in a wide range of motion velocity. A dynamic model proposed by Dahl [19] describes the spring-like behavior during stiction. It is noted that the Dahl model is essentially Coulomb friction with a lag in the change of friction force when the motion direction is changed. In the Dahl model, however, it does not include the Stribeck effect [20], i.e. the effect in which friction force decreases as relative velocity increases in a certain velocity regime. An attempt to extend the Dahl model to include the Stribeck effect was made by Bliman [21]. The drawback of the model by Bliman is that the Stribeck term is present in a spatial representation after a change of the direction of motion, i.e. is not present in the steady-state relation between velocity and friction force. To overcome this drawback, Canudas de Wit et al. [22,23] proposed another dynamic friction model that combines the Dahl effect with arbitrary steady-state friction characteristics including the Stribeck effect. This model by Canudas de Wit et al. was known as the LuGre model. An advantage of the LuGre model is its rich dynamic behavior because it can give possibilities to model properties of presliding displacement, friction lag, varying break-away force and stick-slip motion. The LuGre model is useful for problems of control related to friction force because it has passivity properties, and can give asymptotically stable closed-loop systems [24,25]. There is a lot of works that utilize the LuGre model as a tool for modeling and simulating dynamical systems in engineering [1,26–30].

Recently, there are several modified and extended versions of the LuGre model that are proposed to study different dynamical systems with friction. Al-Bender et al. [31] have investigated a novel generic model at asperity level for dry friction force dynamics. This model can be considered as an upgrade of the LuGre model. The authors have shown many observed phenomena of friction of dynamic systems such as the presliding regime, time-independent frictional hysteresis in the displacement, velocity weakening, slider lift-up effect and frictional lag. Dupont et al. [32,33] proposed an elasto-plastic friction model that is considered as an enhancement of the LuGre model. In this model, under loading, frictional displacement is first purely elastic and then transitions to plastic. The model is demonstrated to preserve the favorable properties of existing models (e.g., dissipativity) and to provide a comparable match to experimental data. Based on the LuGre model, Gonthier et al. [34] have developed a friction model with general regularized contact properties in which the internal state variable is reformulated into two distinct phases: a phase for the stick regime and another for the sliding regime. They introduce a sticking state function as a bridge between the stick-slip friction regimes. The model also includes temporal lag and dwell-time effects. Saha et al. [35] have proposed a new friction model based on the well-known LuGre friction model that can accurately describe the nature of friction force in the gross sliding regime. The advantage of the model by Saha et al. is that it can show both clockwise as well as counter clockwise hysteretic loops in the pure sliding domain. Using the state variable approach, in a recent short communication by Krasmik and Schlattmann [36], the LuGre model is extended to include the effect of frictional aging. In their model, the constant static friction force is replaced by a time-dependent variable representing the variation of the static friction force between a lower limit and an upper limit depending on the stationary contact time. Pikunov and Stefanski [37] have improved the LuGre model by adding weighted coefficients to the governing equation of internal state variable describing the elastic deflection of bristles for surface asperities. These authors have investigated dynamic properties of a friction-induced mechanical oscillator with cubic nonlinearity using their improved version of friction.

In the field of control of engineering systems, various improved versions of the LuGre model can be found, for example, in model of robot control [38–40], in a research on opto-electronic tracking systems [41,42], in a hybrid pump-controlled asymmetric (single-rod) cylinder drive system [43]. From experimental observation, Hideki and Yuta [44] realize that the LuGre model cannot simulate the real friction characteristics of hydraulic actuators. Therefore, the LuGre model is modified taking the dynamics of lubricant film formation into consideration. The lubricant film dynamics is approximated by a first-order lag element and its time constant is varied among the acceleration, deceleration and dwell periods. Based on modified LuGre model by Hideki and Yuta [44], an improved version for modeling dynamic friction of hydraulic cylinders is proposed by Tran et al. [45]. They replace the usual fluid friction term, which is proportional to velocity, with a first-order lead dynamics. This proposed model can give accurate simulation results in the fluid lubrication regime including normal compliance, energy dissipation, and tangential friction. In [46], Deur et al. have suggested several extended versions of the LuGre model for studying dynamic friction model of tyre systems with the aim of improving the model accuracy and applicability in the field of vehicle system dynamics. In [47], Yongjie et al. have presented a modified form of the LuGre model for investigation of vehicle dynamics. The mathematical expression for the modified model is achieved through introducing the Bouc-Wen model to reflect hysteresis effect of the system dynamics. The work by Sobczyk et al. [48] presents a novel continuous approximation of the LuGre model, with the aim of improving its applicability in the control of a class of systems that include fluid-driven servo positioners. The advantage of the proposed approximation is that, it preserves the properties of boundedness and passivity that are inherent to the original LuGre model.

The difference between the static and dynamic friction models is that the dynamic models contain internal state variables that describe hidden quantities, not immediately measurable by macroscopic observations [49]. The number of internal state variables can be increased depending on the friction models in specified fields of engineering applications. To look for and simplify model of real systems, in most cases, one internal state variable is selected because the corresponding identification of system friction parameters is more convenient than that of systems with many internal variables (see: [22,31,50–53]). Recently, a model of two state variables by Ruderman and Bertram [54] has been proposed to describe more precisely behaviors of dynamical systems. They introduce a model with a linear combination of two nonlinear state variables in which one independent and one dependent friction states capture the presliding hysteresis and transient sliding response. Their model has seven parameters. The system model identification is performed under real circumstances of the actuated motion close to the applications with electro-mechanical drives.

An interesting effect is dwell-time in friction phenomena related to the time of contact of two sliding surfaces. The dwell-time is considered as an internal state variable in dynamic friction models. The dwell-time, also called aging time, is interpreted in detail in a research by Baumberger and Berthoud [55,56] for analysis of the state- and rate-dependent friction law. The dwell-time is an important factor in describing dynamics of multicontact interfaces (MCIs) between macroscopic solids with rough surfaces. For non-moving MCIs, the dwell-time is simply the time which has been present at rest. Also for MCIs sliding at a constant velocity, when the motion starts, a given microcontact is gradually sheared until it slides, then disappears as relative motion between surface asperities reaches a value on the order of a faction of the contact diameter [56,57]. The dwell-time effect has a significant influence on friction force in the case of low velocity of system motion, and it must be included in friction model used for problem of friction compensation [58,59]. In [56], Baumberger and Berhhoud have presented a physical analysis of dynamic friction at nonlubricated multicontact interfaces between nominally flat bodies, rough on the micrometer scale, made of identical polymer glasses. The model of state-dependent friction is described by a first-order governing equation of the dwell-time variable. Differing from the LuGre model [22], the model by Baumberger and Berhhoud [56] has friction coefficient in the form of logarithm law similar to the Rice-Ruina state- and rate-dependent friction model [60]. Recently, from the idea on the presence of dwell-time in engineering systems with stick-slip motion, Simoni et al. [61] have proposed a two-

state friction model that can be considered as a combination of the LuGre model [22] and the modified Dieterich-Ruina model [60,62]. Simoni et al. show that this model of friction can capture many friction phenomena such as the presliding, stick-slip behavior, the rate-dependent and dwell-time effect. We have found that the model by Simoni et al. is a new model and may have a potential of applications for a wide range of engineering problems because it can cover the advantages of both the LuGre and Dieterich-Ruina models. This has motivated us to study the Simoni's model further by approaching both theoretical and numerical researches. According to the works of Baumberger et al. and Simoni et al. [56,57,61], the meaning of the term "dwell-time" used in this study is average time elapsed since the contacts existing at a given instant were first formed.

The objective of our study is to develop the two-state friction model to the problem of stick-slip motion of a system placed on a belt moving at constant speed. Our attention is focused on the range of low velocity of motion to capture the dwell-time effect. This is important problem in engineering because it relates to issues of precise control at near-zero velocity range and the stick-slip phenomenon is often observed in the case of motion between two surfaces with low velocity. Characteristics of system motion are explored in detail.

2. Model of friction with two internal state variables

2.1. LuGre model

The LuGre model is an extended version of the Dahl model that can capture the Stribeck effect at low-velocity. In fact, contact surfaces are very irregular at the microscopic scale and make contact at a number of asperities. From the assumption of surface elastic contact, the surface asperities are modeled as elastic bristles. When applying a tangential force, bristles will deflect like springs and give rise to the friction force. Canudas de Wit et al. [22] proposed a friction model based on the average deflection behavior of bristles. The average deflection of bristles is denoted as z, namely, internal state variable, and is modeled by the following equation:

$$\dot{z} = v - \frac{\sigma_0 |v|}{g(v)} z, \tag{1}$$

where v is the relative velocity between two surfaces; σ_0 is stiffness coefficient. The Stribeck function of relative velocity $g = g(v)$, is given by

$$g(v) = c_0 + c_s \exp\{-\alpha |v|\}, \tag{2}$$

where c_0 is the Coulomb friction force, c_s is the difference between static and Coulomb friction forces, α is a constant. It is seen that the function $g(v)$ approaches c_0 as the relative velocity v tends to infinity, i.e. the LuGre model is reduced to the Dahl model. In contrast, when relative velocity v tends to zero, the function $g(v)$ reaches to a static friction force. The Stribeck effect is present this near-zero velocity range. The friction expression in the LuGre model is constituted from three components: elastic term $\sigma_0 z$, damping characteristic term of internal state variable, $\sigma_1 \dot{z}$, and viscous force term, $f(v) = c_1 v$

$$F_{fr} = \sigma_0 z + \sigma_1 \dot{z} + c_1 v, \tag{3}$$

where constants σ_1, c_1 are internal damping and viscous damping coefficients. The first two are related to the internal variable z whereas the third coefficient exhibits the relative motion between two surfaces. It is noted that the functions f and g can be chosen to match a set of steady-state friction measurement data. In most previous studies, the function $f(v)$ is chosen as a linear function of relative velocity v whereas function g takes a specified shape depending on the exponent term $\exp\{-\alpha |v|^s\}$ with s being a real number, for example, Simoni et al. [61] selected $s = 1$, Canudas de Wit et al. [22] suggested $s = 2$ for the LuGre model. The addition of the state variable z makes the LuGre model overcome the major limit of Dahl model, that is, the possibility to present the static friction state in the presliding regime.

In the steady-state regime of bristle motion, i.e. $\dot{z} = 0$, the average deflection z is given by

$$z_{ss} = g(v)\text{sgn}(v)/\sigma_0. \tag{4}$$

Therefore, the friction force at the steady-state regime is

$$F_{fr} = g(v)\text{sgn}(v) + c_1 v. \tag{5}$$

This model is reduced to the Coulomb model in the case $g(v) = c_0$ and $f(v) = 0$.

2.2. Dwell-time as a new internal state variable

The main disadvantage of the LuGre model is that it does not include the dwell-time effect, that is, it can not model the variation of friction force when two surfaces are kept in contact, at rest, for a certain time. We denote the dwell-time as a new internal state variable, ϕ. It can be considered as the aging time [55,56], that is the mount of time during which the two surfaces are kept in contact with zero-relative velocity. Simoni et al. [61] have proposed a model established based on a combination of two models, namely, the LuGre [22] and Dieterich-Ruina models [60,62]. The Dieterich-Ruina model is a dynamic friction one developed in the field of geophysics that can capture how friction between two rock layers increases with dwell-time. In this model, the friction force depends both on the instantaneous sliding velocity $\dot{x}$ and on the aging time variable ϕ. Similarly, an approach for the model of two internal state variables by Simoni et al. [61] is that the friction force is added by a component related to the aging time while components of LuGre model are retained:

$$F_{fr} = \sigma_0 z\left[1 + a\left(1 - \exp\left\{-\phi/\phi_0\right\}\right)\right] + \sigma_1 \dot{z} + f(v), \tag{6}$$

where ϕ_0 is a positive parameter, a is positive dimensionless parameter [55,62]. In Eq. 6, two internal state variables z and ϕ are present. The first variable related to the deflection of bristles plays the role of capturing friction effect of pre-sliding motion whereas the second one models the effect of dwell-time between two surfaces in contact. The internal state z governed by Eq. 1 is the same as in the LuGre model. The aging time ϕ is determined from the first-order differential equation with coefficient depending on the velocity variable v

$$\dot{\phi} = 1 - \frac{|v|}{D_0}\phi. \tag{7}$$

In [55,56], the variable ϕ can be interpreted as the age of the multi-contact interfaces (MCI), i.e. as time average elapsed since the contacts existing at a given instant were first formed. It is noted that at the steady-state regime of motion with a certain velocity V, contacts are destroyed and replaced by a non-correlated set of fresh ones after sliding a length D_0 so that $\phi = D_0/V$. At non-stationary motion, the variable ϕ is a function of time that keeps to track the previous slip history on the finite sliding length D_0. When the velocity is equal to zero, Eq. (7) behaves as a unit integrator, that is, in this case, $\phi = t$ with initial condition $\phi(0) = 0$. This simple case reveals that the dwell-time increases with time as relative velocity between two surfaces tends to zero. This leads to the fact that friction force between two surfaces in contact is varying in time and depends on the internal state variable ϕ.

The Simoni's area term $s_t = a\left(1 - \exp\left\{-\phi/\phi_0\right\}\right)$ can be interpreted as a true contact area (recall a is a dimensionless quantity) between two surfaces in contact [61]. Its value is increasing with the growth of the dwell-time ϕ. As ϕ tends to its maximum value, the true contact area approaches to a limit value s_L. In case of very large value of ϕ, the contact area approaches to value a i.e. the friction force generated from the dwell-time effect is bounded by $\sigma_0 z_{\max} a$ where $z_{\max}$ is the maximum deflection of bristles.

Because the dwell-time variable ϕ is coupled with the relative velocity v, the presence of ϕ in the model will affect the quasi-zero velocity term $g(v)$ in the LuGre model.

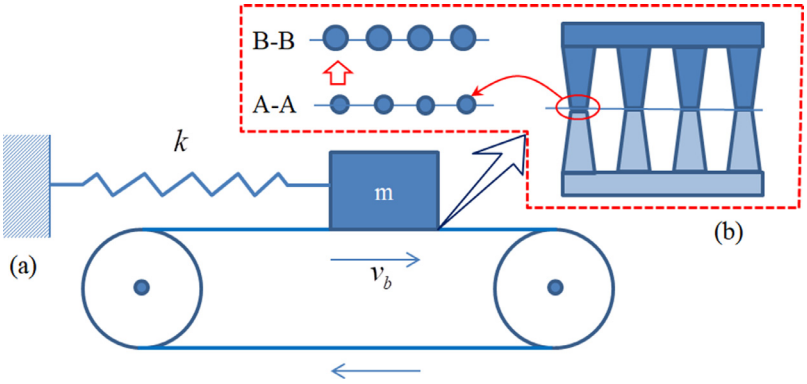

Fig. 1. Model of mass block traveling on a belt and model of contact surfaces as bristles with variation of true contact area from the beginning A-A to the end B-B of dwell-time interval.

The exploration of the influence of dwell-time on characteristics of sliding motion, presliding motion, stick-slip motion and rate-dependence of a simple system is studied in detail in a recent paper by Simoni et al. [61]. The model by Simoni et al. has promising potential for exploring other engineering systems because it takes advantage of LuGre model associated with that of Dieterich-Ruina model in which friction characteristics have been verified from experimental data. In the following section, we develop the model by Simoni et al. to a problem of mass block moving on a belt in which stick-slip motion is observed at low-velocity. Effects related to dwell-time are examined numerically and clarified.

3. Model of spring-mass system with dwell-time effect

Consider a model of mass block traveling on a belt moving at constant speed v_b, as shown in Fig. 1a. The mass block connects to a fixed wall by a spring with stiffness k. When moving, the mass contacts with surface of the belt. The contact surfaces are modeled as elastic bristles as described in Sect. 2. Using model proposed by Simoni et al. [61], the true contact area between surfaces varies from the beginning state A-A to the end state B-B of the dwell-time interval, as illustrated in Fig. 1b. The governing equations of the system are written as:

$$m\ddot{x} = -kx + \sigma_0 z\left[1 + a\left(1 - \exp\left\{-\phi/\phi_0\right\}\right)\right] + \sigma_1 \dot{z} + c_1\left(v_b - \dot{x}\right), \tag{8a}$$

$$\dot{z} = \left(v_b - \dot{x}\right) - \frac{\sigma_0\left|v_b - \dot{x}\right|}{g\left(v_b - \dot{x}\right)} z, \tag{8b}$$

$$\dot{\phi} = 1 - \frac{\left|v_b - \dot{x}\right|}{D_0}\phi, \tag{8c}$$

where relative velocity between the mass and belt is $v_r = v_b - \dot{x}$; $g\left(v_b - \dot{x}\right)$ is determined based on Eq. (2) for relative velocity $v_b - \dot{x}$ as follows

$$g\left(v_b - \dot{x}\right) = c_0 + c_s \exp\left\{-\alpha\left|v_b - \dot{x}\right|\right\}. \tag{9}$$

In the right-hand side of Eq. (8a), the first term is spring force, $F_{sp} = kx$; the second term contains two components: the component $\sigma_0 z$ is the elastic force of internal variable z, the remaining component $\sigma_0 a\left(1 - \exp\left\{-\phi/\phi_0\right\}\right)z$ coupled with the variable z is generated from the consideration of effect of the dwell-time during contact of two surfaces; the third and forth terms are related to the damping of internal variable state and viscous damping of mass block motion, respectively. If $\dot{x}$ is approximate with the belt velocity v_b, the contribution of viscous damping force $c_1\left(v_b - \dot{x}\right)$ is not considerable.

3.1. Equilibrium point and added displacement due to dwell-time effect

The equilibrium point of the system is obtained when derivatives of all system state variables in time vanishes, i.e. $\dot{x} = 0,\ \ddot{x} = 0,\ \dot{z} = 0,\ \dot{\phi} = 0$. This leads to the following equation for finding equilibrium point $\left\{x_e,\ z_e,\ \phi_e\right\}$:

$$-kx + \sigma_0 z\left[1 + a\left(1 - \exp\left\{-\phi/\phi_0\right\}\right)\right] + c_1 v_b = 0,$$

$$v_b - \frac{\sigma_0\left|v_b\right|}{g\left(v_b\right)} z = 0,$$

$$1 - \frac{\left|v_b\right|}{D_0}\phi = 0,$$

where $g\left(v_b\right) = c_0 + c_s \exp\left\{-\alpha v_b\right\}$. Solving this system with the assumption of positive belt velocity $v_b > 0$, we obtain $\left\{x_e,\ z_e,\ \phi_e\right\}$

$$x_e = \frac{g\left(v_b\right)\left[1 + a\left(1 - \exp\left\{-\phi_e/\phi_0\right\}\right)\right] + c_1 v_b}{k}, \tag{11a}$$

$$z_e = \frac{g\left(v_b\right)}{\sigma_0}, \tag{11b}$$

$$\phi_e = \frac{D_0}{v_b}. \tag{11c}$$

Eq. (11c) shows that the equilibrium value of dwell-time variable is different from zero and is positive. In the case of dwell-time depending on time t, it is shown that $\phi(t)$ is positive for all time because at a certain critical time point t_{cr} if exists, the function $\phi(t)$ gets minimum value $\phi_{cr} = D_0/\left|v\left(t_{cr}\right)\right|$ and this value is positive.

It is emphasized that the values z_e and ϕ_e are, respectively, identical with values z_{ss} and ϕ_{ss} at the sliding steady-state of system motion in which derivatives of internal state variables z, ϕ reach to zero at large relative velocity of mass block on belt. This is because, at large relative velocity, the bristle deflection tends to a limit value and the sliding regime starts. The meaning of D_0 is the finite sliding length, the quantity ϕ_e has the meaning of sliding time of surface at sliding velocity v_b of the belt. If keeping parameter D_0 at fixed value, the increase of belt speed will make the dwell-time ϕ_e shorter.

From Eq. (11b), the product $g\left(v_b\right) = \sigma_0 z_e$ shows that value of function $g(v)$ at the velocity v_b is the friction force corresponding to the elastic part of bristles at equilibrium state. It is easy seen that $c_0 \le g \le c_0 + c_s$, where the lower bound c_0 is the Coulomb friction force and the upper bound $c_0 + c_s$ is the static friction force. These inequalities for the function g lead to the fact that the response z_e at equilibrium state is bounded in the interval $c_0/\sigma_0 \le z_e \le \left(c_0 + c_s\right)/\sigma_0$. Moreover, the evolution response of z in time t also satisfies $c_0/\sigma_0 \le |z(t)| \le \left(c_0 + c_s\right)/\sigma_0$. This property of boundedness of average deflection of bristle is confirmed by Canudas de Wit et al. [22,23] using the Lyapunov function method.

From the relationship of responses z_e, ϕ_e and belt velocity v_b, one can express equilibrium deflection z_e via the dwell-time ϕ_e as follows

$$\sigma_0 z_e = g\left(\frac{D_0}{\phi_e}\right) = c_0 + c_s \exp\left\{-\frac{\alpha D_0}{\phi_e}\right\}. \tag{12}$$

As mentioned above, the product $F_{\text{elastic,e}} = \sigma_0 z_e$ is value with respect to elastic component of friction force at equilibrium state. In this situation, the friction is monotonically increasing with the finite dwell-time value ϕ_e. This means the dwell-time will affect friction force, it makes friction increase if two surfaces are kept in contact in a certain time interval.

The expression (11a) for the equilibrium displacement response x_e is different from that obtained by the LuGre model because of the contribution of an added displacement component $x_{e,\text{dw}}$ generated by the dwell-time effect:

$$x_{e,\text{dw}} = \frac{ag(v_b)\left(1-\exp\left\{-\phi_e/\phi_0\right\}\right)}{k}. \tag{13}$$

Substituting the expression of $g(v_b)$ and dwell-time ϕ_e from Eq. (11c) into Eq. (13), we obtain

$$x_{e,\text{dw}} = \frac{ac_0}{k}\left(1+\frac{c_s}{c_0}\exp\left\{-\alpha v_b\right\}\right)\left(1-\exp\left\{-\frac{D_0}{\phi_0 v_b}\right\}\right). \tag{14}$$

Eq. (14) shows the dependence of the added displacement $x_{e,\text{dw}}$ on the belt velocity. The quantity c_0/k can be considered as a displacement of a unit mass with the pulling force being equal to the Coulomb friction force. The displacement ac_0/k obtained from displacement c_0/k by a scale coefficient a that plays role of true contact area of two surfaces in contact. In Eq. (14), the first dimensionless component $1+\left(c_s/c_0\right)\exp\left\{-\alpha v_b\right\}$ is the contribution of the Stribeck effect whereas the second component $1-\exp\left\{-D_0/\left(\phi_0 v_b\right)\right\}$ is produced from the result of dwell-time effect. In the cases of limit, if belt velocity tends to infinity, both the Stribeck and dwell-time effects disappears, and therefore, the added displacement is equal zero:

$$\lim_{v_b\to+\infty} x_{e,\text{dw}} = 0. \tag{15}$$

In near-zero range of the belt velocity, it is seen from Eq. (11c) that the dwell-time ϕ_e is very large. Therefore, the exponential term $\exp\left\{-D_0/\left(\phi_0 v_b\right)\right\}$ is approximate to zero whereas the term $\exp\left\{-\alpha v_b\right\}$ is near unit value. As a consequence, the limit of added displacement is

$$\lim_{v_b\to 0} x_{e,\text{dw}} = \frac{ac_0}{k}\left(1+\frac{c_s}{c_0}\right). \tag{16}$$

If we consider $x_{e,\text{dw}}$ as a function of velocity v_b, it can be shown that the function $x_{e,\text{dw}}$ is monotonically decreasing with respect to variable v_b. Hence, the value of $x_{e,\text{dw}}$ is bounded in a range with lower bound determined from (15) and upper bound determined from (16):

$$0 \le x_{e,\text{dw}} \le \frac{ac_0}{k}\left(1+\frac{c_s}{c_0}\right). \tag{17}$$

The equilibrium point in Eq. (11) can be stable or unstable depending on the determination range of system parameters. In the following subsection, the Routh-Hurwitz criterion is used to examine the stability of the equilibrium point and effects of dwell-time on the stable property of the system.

3.2. Stability conditions of equilibrium point via Routh-Hurwitz criterion

The system (8 a,b,c) is rewritten as

$$\begin{aligned}
\dot{x} &= Q_1(x,y,z,\phi) := y,\\
\dot{y} &= Q_2(x,y,z,\phi) := -\frac{k}{m}x + \frac{\sigma_0}{m}z\left[1+a\left(1-\exp\left\{-\phi/\phi_0\right\}\right)\right]\\
&\quad + \frac{\sigma_1}{m}\left[\left(v_b-y\right)-\sigma_0 z h\left(v_b-y\right)\right] + \frac{c_1}{m}\left(v_b-y\right),\\
\dot{z} &= Q_3(x,y,z,\phi) := \left(v_b-y\right)-\sigma_0 z h\left(v_b-y\right),\\
\dot{\phi} &= Q_4(x,y,z,\phi) := 1-\frac{\left|v_b-y\right|}{D_0}\phi,
\end{aligned} \tag{18}$$

where $h(v)=|v|/g(v)$ is a function of velocity argument v; $Q_j = Q_j(x,y,z,\phi)$ (j=1,2,3,4) are nonlinear functions of state vector variable $\mathbf{w}=[x\ \ y\ \ z\ \ \phi]^T$. To analyze properties of stability of the system (18), we linearize this system in neighborhood of the equilibrium point of state vector variable, i.e. the point $\mathbf{w}_e = \begin{bmatrix} x_e & 0 & z_e & \phi_e \end{bmatrix}^T$. Denote $\tilde{x} = x - x_e$, $\tilde{y} = y - 0$, $\tilde{z} = z - z_e$, $\tilde{\phi} = \phi - \phi_e$ as disturbances of state vector components around the equilibrium point $\mathbf{w}_e$. The linearized equation system takes the following form

$$\dot{\tilde{\mathbf{w}}} = \mathbf{J}\left(\mathbf{w_e}\right)\tilde{\mathbf{w}}, \tag{19}$$

where $\mathbf{J}\left(\mathbf{w}_e\right)$ is the Jacobian matrix of nonlinear vector $\mathbf{Q} = \begin{bmatrix} Q_1 & Q_2 & Q_3 & Q_4 \end{bmatrix}^T$ calculated at the point $\mathbf{w}_e$:

$$\mathbf{J}\left(\mathbf{w}_e\right) = \begin{bmatrix} 0 & 1 & 0 & 0\\ j_{21} & j_{22} & j_{23} & j_{24}\\ 0 & j_{32} & j_{33} & 0\\ 0 & j_{42} & 0 & j_{44} \end{bmatrix}, \tag{20}$$

where 8 elements of the matrix $\mathbf{J}$ are displayed in which they contain system parameters, other elements are either equal to zero or one:

$$\begin{aligned}
j_{21} &= -\frac{k}{m},\\
j_{22} &= \frac{\alpha\sigma_1 c_s}{m}h\left(v_b\right)\exp\left\{-\alpha v_b\right\} - \frac{c_1}{m},\\
j_{23} &= \frac{\sigma_0}{m}\left[1+a\left(1-R\left(v_b\right)\right)\right] - \frac{\sigma_0\sigma_1}{m}h\left(v_b\right),\\
j_{24} &= \frac{a}{m\phi_0}g\left(v_b\right)R\left(v_b\right),\\
j_{32} &= \alpha c_s h\left(v_b\right)\exp\left\{-\alpha v_b\right\},\\
j_{33} &= -\sigma_0 h\left(v_b\right),\\
j_{42} &= \frac{1}{v_b},\\
j_{44} &= -\frac{v_b}{D_0},
\end{aligned} \tag{21}$$

where $h\left(v_b\right) = v_b/g\left(v_b\right)$; the term $R = R\left(v_b\right) = \exp\left\{-D_0/\left(\phi_0 v_b\right)\right\}$ is related to the true contact area $a(1-R)$ between two surfaces. In this representation, R is a function of the parameter v_b and also depends on two parameters of dwell-time effect, D_0, ϕ_0. The characteristic polynomial of the matrix (20) is given by

$$\lambda^4 + b_3\lambda^3 + b_2\lambda^2 + b_1\lambda + b_0 = 0, \tag{22}$$

where coefficients of the polynomial are determined as follows

$$\begin{aligned}
b_3 &= -\left(j_{22}+j_{33}+j_{44}\right),\\
b_2 &= j_{22}j_{33} + j_{22}j_{44} + j_{33}j_{44} - j_{23}j_{32} - j_{24}j_{42} - j_{21},\\
b_1 &= -j_{22}j_{33}j_{44} + j_{23}j_{32}j_{44} + j_{24}j_{42}j_{33} + j_{33}j_{21} + j_{44}j_{21},\\
b_0 &= -j_{33}j_{44}j_{21}.
\end{aligned} \tag{23}$$

Substituting elements j_{rs} from Eqs. (21) into Eqs. (23) and collecting expressions b_i $(i=1,2,3,4)$ in terms of dimensionless quantity αv_b, we obtain

$$\begin{aligned}
b_3 &= \frac{\sigma_0}{\alpha c_0}\tilde{b}_3\left(v_b,\ k,\ c_1\right),\\
b_2 &= \frac{k}{m}\tilde{b}_2\left(v_b,\ k,\ c_1\right),\\
b_1 &= \frac{k}{m}\frac{\sigma_0}{\alpha c_0}\tilde{b}_1\left(v_b,\ k,\ c_1\right),\\
b_0 &= \left(\frac{k}{m}\right)^2\tilde{b}_0\left(v_b,\ k,\ c_1\right),
\end{aligned} \tag{24}$$

where $\tilde{b}_3,\ \tilde{b}_2,\ \tilde{b}_1,\ \tilde{b}_0$ are dimensionless coefficients determined as follows

$$\begin{aligned}
\tilde{b}_3 &= \frac{\alpha v_b}{1+\mu_s \exp\{-\alpha v_b\}}\left[1-\frac{\alpha\sigma_1 c_s}{m\sigma_0}\exp\{-\alpha v_b\}\right]+\frac{c_0}{\sigma_0 D_0}(\alpha v_b)+\frac{(\alpha c_0)^2}{m\sigma_0}\frac{c_1}{\alpha c_0},\\
\tilde{b}_2 &= 1-\frac{c_s}{c_0}\frac{\sigma_0}{k}\left[\frac{\sigma_1}{\alpha c_0}\frac{c_0}{\sigma_0 D_0}(\alpha v_b)+1+a\big(1-R(v_b)\big)\right]\frac{\alpha v_b\exp\{-\alpha v_b\}}{1+\mu_s\exp\{-\alpha v_b\}}\\
&\quad+\frac{\sigma_0}{k}\left(\frac{c_1}{\alpha c_0}+\frac{m\sigma_0}{\alpha^2 c_0^2}\frac{c_0}{\sigma_0 D_0}(\alpha v_b)\right)\frac{\alpha v_b}{1+\mu_s\exp\{-\alpha v_b\}}\\
&\quad-\frac{a\alpha c_0}{\sigma_0\phi_0}\frac{\sigma_0}{k}\frac{1+\mu_s\exp\{-\alpha v_b\}}{\alpha v_b}R(v_b)+\frac{c_1}{\alpha c_0}\frac{c_0}{\sigma_0 D_0}\frac{\sigma_0}{k}(\alpha v_b),\\
\tilde{b}_1 &= -\frac{c_s}{c_0}\frac{c_0}{\sigma_0 D_0}\frac{\sigma_0}{k}(\alpha v_b)\\
&\quad\times\left\{\big[1+a\big(1-R(v_b)\big)\big]\frac{\alpha v_b\exp\{-\alpha v_b\}}{1+\mu_s\exp\{-\alpha v_b\}}-\frac{c_0}{c_s}\frac{c_1}{\alpha c_0}\frac{\alpha v_b}{1+\mu_s\exp\{-\alpha v_b\}}\right\}\\
&\quad-\frac{a\alpha c_0}{\sigma_0\phi_0}\frac{\sigma_0}{k}R(v_b)+\frac{\alpha v_b}{1+\mu_s\exp\{-\alpha v_b\}}+\frac{c_0}{\sigma_0 D_0}(\alpha v_b),\\
\tilde{b}_0 &= \frac{m\sigma_0}{\alpha^2 c_0^2}\frac{\sigma_0}{k}\frac{c_0}{\sigma_0 D_0}\frac{(\alpha v_b)^2}{1+\mu_s\exp\{-\alpha v_b\}},
\end{aligned}\tag{25}$$

where $\mu_s = c_s/c_0$. In (25), we collect original system parameters into a set of dimensionless parameters, $\mathfrak{F}$,

$$\mathfrak{F}=\left\{\alpha v_b,\quad \mu_s,\quad \frac{\alpha\sigma_1 c_s}{m\sigma_0},\quad \frac{c_0}{\sigma_0 D_0},\quad \frac{\alpha^2 c_0^2}{m\sigma_0},\quad \frac{c_1}{\alpha c_0},\quad \frac{\sigma_0}{k},\quad \frac{\sigma_1}{\alpha c_0},\quad \frac{a\alpha c_0}{\sigma_0\phi_0}\right\}.\tag{26}$$

Here, we consider coefficients $\tilde{b}_3,\ \tilde{b}_2,\ \tilde{b}_1,\ \tilde{b}_0$ as functions of three interested arguments $v_b,\ k,\ c_1$ in our numerical investigation of stability analysis.

The Routh-Hurwitz criterion [63–66] implies that the equilibrium point $\mathbf{w_e}$ is asymptotically stable if and only if coefficients b_i, $(i = 1,2,3,4)$ satisfy the following conditions:

$$\begin{aligned}
&b_0>0,\ \ b_3>0,\\
&\frac{b_2b_3-b_1}{b_3}>0,\\
&\frac{(b_2b_3-b_1)b_1-b_3^2b_0}{b_2b_3-b_1}>0.
\end{aligned}\tag{27}$$

Substitution of (24) into (27) yields

$$\begin{aligned}
&\varsigma_1=\tilde{b}_0>0,\\
&\varsigma_2=\tilde{b}_3>0,\\
&\varsigma_3=\frac{\tilde{b}_2\tilde{b}_3-\tilde{b}_1}{\tilde{b}_3}>0,\\
&\varsigma_4=\frac{(\tilde{b}_2\tilde{b}_3-\tilde{b}_1)\tilde{b}_1-\tilde{b}_3^2\tilde{b}_0}{\tilde{b}_2\tilde{b}_3-\tilde{b}_1}>0,
\end{aligned}\tag{28}$$

where we denote ς_i $(i = 1,2,3,4)$ as functions of system parameters. It is easily seen that the condition $\varsigma_1=\tilde{b}_0>0$ is obvious. The condition $\varsigma_2=\tilde{b}_3>0$ gives:

$$\begin{aligned}
&\frac{\alpha v_b}{1+\mu_s\exp\{-\alpha v_b\}}\left[1-\frac{\alpha\sigma_1 c_s}{m\sigma_0}\exp\{-\alpha v_b\}\right]\\
&+\frac{c_0}{\sigma_0 D_0}(\alpha v_b)+\frac{(\alpha c_0)^2}{m\sigma_0}\frac{c_1}{\alpha c_0}>0
\end{aligned}\tag{29}$$

We assume that the magnitude of parameter σ_0 is enough large in comparison with that of parameters $\alpha,\ \sigma_1,\ c_s$ so that the inequality $\alpha\sigma_1 c_s/(m\sigma_0)\ll 1$ holds. The inequality $\exp\{-\alpha v_b\}\le 1$ holds for all positive velocity v_b. From these inequalities, we have $\alpha\sigma_1 c_s/(m\sigma_0)\exp\{-\alpha v_b\}<1$. Consequently, the condition $\tilde{b}_3>0$ is fulfilled.

Due to the complicated expressions of the remaining conditions in (28), they are not been displayed here. Characteristics of stability are checked via numerical calculations in Section 4.

3.3. Stability conditions for the case of LuGre model

When the dwell-time is not considered, Eq. (22) is reduced to the LuGre model and the corresponding characteristic polynomial equation is given by:

$$\lambda^3+l_2\lambda^2+l_1\lambda+l_0=0,\tag{30}$$

where

$$l_2=\frac{k}{m}\tilde{l}_2(v_b,\,k,\,c),\ \ l_1=\frac{k}{m}\frac{\sigma_0}{\alpha c_0}\tilde{l}_1(v_b,\,k,\,c),\ \ l_0=\left(\frac{k}{m}\right)^2\tilde{l}_0(v_b,\,k,\,c)\tag{31}$$

with $\tilde{l}_i$ $(i=1,2,3)$ being dimensionless coefficients defined as follows

$$\begin{aligned}
\tilde{l}_2 &= \frac{\alpha v_b}{1+\mu_s\exp\{-\alpha v_b\}}\left[1-\frac{\alpha\sigma_1 c_s}{m\sigma_0}\exp\{-\alpha v_b\}\right]\\
&\quad+\frac{(\alpha c_0)^2}{m\sigma_0}\frac{c_1}{\alpha c_0},\\
\tilde{l}_1 &= 1-\frac{c_s}{c_0}\frac{\sigma_0}{k}\frac{\alpha v_b\exp\{-\alpha v_b\}}{1+\mu_s\exp\{-\alpha v_b\}}\\
&\quad+\frac{\sigma_0}{k}\frac{c_1}{\alpha c_0}\frac{\alpha v_b}{1+\mu_s\exp\{-\alpha v_b\}},\\
\tilde{l}_0 &= \frac{\alpha v_b}{1+\mu_s\exp\{-\alpha v_b\}}.
\end{aligned}\tag{32}$$

It is observed that the expressions $\tilde{l}_2,\tilde{l}_1,\tilde{l}_0$ from (32) are obtained from (25) by removing terms related to parameters $D_0,\ \phi_0,\ a$ of dwell-time effect in the expressions $\tilde{b}_3,\tilde{b}_2,\tilde{b}_1$, respectively.

The condition for stability of the LuGre model is

$$\begin{aligned}
&l_0>0,\ \ l_2>0,\\
&l_1l_2-l_0>0.
\end{aligned}\tag{33}$$

The substitution of (31) into (33) yields

$$\begin{aligned}
&\tilde{l}_0>0,\ \ \tilde{l}_2>0,\\
&\tilde{l}_1\tilde{l}_2-\tilde{l}_0>0.
\end{aligned}\tag{34}$$

Assume that the inequality $\alpha\sigma_1 c_s/(m\sigma_0)\ll 1$ holds, as presented in (29) for the two-state model, we also have $\tilde{l}_2>0$. The stability condition of equilibrium point of the LuGre model is now dependent on the third condition in (34), i.e. $\tilde{l}_1\tilde{l}_2-\tilde{l}_0>0$. This condition will be checked numerically in the Section 4.

3.4. Hopf bifurcation

A Hopf bifurcation analysis is necessary to identify the appearance or disappearance of a periodic orbit through a local change in the stability properties of a fixed point of nonlinear dynamical systems [68,69]. The bifurcated limit cycles can be observed in phase space of dynamical systems. In the traditional approach, the Hopf bifurcation is stated in terms of the properties of eigenvalues in which a pair of complex conjugate eigenvalues of the Jacobian matrix pass through the imaginary axis while all other eigenvalues have negative real parts [67]. This approach is convenient in cases eigenvalues can be found explicitly. To check the existence of Hopf bifurcation of system (18), however, we use another equivalent implicit algorithm criterion of Hopf bifurcation developed by Liu [70], called Liu's criterion, on the basis of the Routh-Hurwitz stability criterion, which is stated in terms of the coefficients of the characteristic equations instead of those of eigenvalues. Applying the Liu's criterion [70] to the characteristic polynomial (22), we have

the following conditions for the occurrence of Hopf bifurcation with bifurcation parameters v_b:

$$(L1): \quad b_0 > 0,\ b_3 > 0,\ b_2 b_3 - b_1 > 0,\ b_1 b_2 b_3 - b_0 b_3^2 - b_1^2 = 0 \tag{35}$$

$$(L2): \quad \frac{d}{dv_b}\left(b_1 b_2 b_3 - b_0 b_3^2 - b_1^2\right) \neq 0 \tag{36}$$

where the coefficients b_3, b_2, b_1, b_0 are determined from (23). Using the transformation of coefficients (24), the conditions (L1) and (L2) can be rewritten in terms of dimensionless coefficients $\tilde{b}_3,\ \tilde{b}_2,\ \tilde{b}_1,\ \tilde{b}_0$ as follows

$$(L1): \quad \tilde{\varsigma}_1 = \tilde{b}_0 > 0,\ \tilde{\varsigma}_2 = \tilde{b}_3 > 0,\ \tilde{\varsigma}_3 = \tilde{b}_2\tilde{b}_3 - \tilde{b}_1 > 0,$$
$$\tilde{\varsigma}_4 = \tilde{b}_1\tilde{b}_2\tilde{b}_3 - \tilde{b}_0\tilde{b}_3^2 - \tilde{b}_1^2 = 0 \tag{37}$$

$$(L2): \quad \frac{d}{dv_b}\left(\tilde{\varsigma}_4\right) \neq 0 \tag{38}$$

It is noted that the condition (L2) also can be applied to other bifurcation parameters of the system. Three conditions $\tilde{b}_0 > 0,\ \tilde{b}_3 > 0,\ \tilde{b}_2\tilde{b}_3 - \tilde{b}_1 > 0$ are shown as similar to that in (28) for Routh-Hurwitz criterion. The fourth condition $\tilde{\varsigma}_4 = \tilde{b}_1\tilde{b}_2\tilde{b}_3 - \tilde{b}_0\tilde{b}_3^2 - \tilde{b}_1^2 = 0$ is equivalent to the equation $\varsigma_4 = \varsigma_4(v_b) = 0$ where ς_4 is determined from (28) because if removing the denominator term from ς_4, the equation $\tilde{\varsigma}_4 = 0$ is obtained. The condition (L2) is checked by numerical calculation as presented in Section 4. We are interested in the equation $\tilde{\varsigma}_4 = 0$ for which a relationship between system parameters is formed, for example, the relation $\tilde{\varsigma}_4(v_b, k, c_1) = 0$ for the belt velocity v_b, stiffness k and damping coefficient c_1. The picture of Hopf bifurcation for the system (18) is illustrated in Fig. 11.

4. Numerical simulations and analysis

4.1. Stable and unstable zones with dwell-time effect

Stable and unstable zones of equilibrium point in the plane of a certain pair of system parameters are formulated based on solving inequalities obtained from the Routh-Hurwitz criterion (28) for the present two-state model and (34) for the LuGre model. As shown before in (29), the system of inequalities (28) gives $\varsigma_1 > 0,\ \varsigma_2 > 0$. The inequalities $\varsigma_3 > 0,\ \varsigma_4 > 0$ are checked by numerical calculations for various values of system parameters. Here, we are interested in three parameters: the belt velocity v_b, viscous damping coefficient c_1, and stiffness k. Because the parameter v_b contributes the change of relative velocity between surfaces of mass element and belt, in this study, the phenomenon of stick-slip motion of the mass block on the belt will be observed with the consideration of dwell-time effect in our model. The parameter c_1 contributes the viscous damping effect of friction force. The viscous effect on the stability of the equilibrium point is considerable if the parameter c_1 has a enough large value. The stiffness parameter k is a scale factor of the elastic force acting on the mass block. During motion there is an exchange of energy between elastic energy potential of spring and energy dissipation of friction force, and therefore the exploration of effect of stiffness k will be considered in our numerical analysis.

For a set of system parameters, the stable state of equilibrium point can be reached if belt velocity v_b lies on an appropriate range that satisfies the condition of Routh-Hurwitz criterion. Fig. 2 portrays graphs of curves $\varsigma_2 = \varsigma_2(v_b),\ \varsigma_3 = \varsigma_3(v_b)$ with the viscous damping coefficient $c_1 = 0.5\ \left(\mathrm{Nsm}^{-1}\right)$. The calculation parameters are given in Table 1. The functions $\varsigma_2,\ \varsigma_3$ increase monotonically and larger than zero for all positive value v_b. The positive value of ς_2 is confirmed from analytical expression (29) whereas that of ς_3 is shown by the numerical illustration in Fig. 2. Fig. 3 exhibits the behavior of function $\varsigma_4 = \varsigma_4(v_b)$ with various values of viscous damping coefficient c_1. The function ς_4 is positive if v_b is larger than a value $v_{b,ZP}$ that is a zero-point of Eq. $\varsigma_4(v_b) = 0$. The solution $v_{b,ZP}$ is obtained using the Newton-Raphson

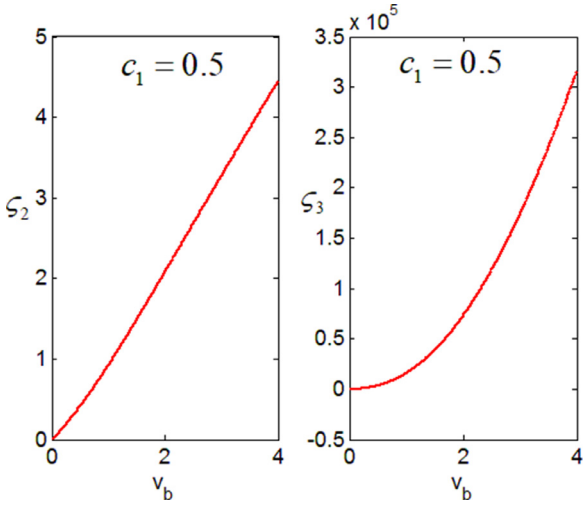

Fig. 2. Graphs of curves $\varsigma_2 = \varsigma_2(v_b),\ \varsigma_3 = \varsigma_3(v_b)$ with the viscous damping coefficient $c_1 = 0.5$.

Table 1
Parameters used in simulation.

Description/Unit	Notation	Value
Spring stiffness (Nm^{-1})	k	100
Mass (kg)	m	1
Internal stiffness (Nm^{-1})	σ_0	60,000
Internal damping (Nsm^{-1})	σ_1	2
Viscous damping (Nsm^{-1})	c_1	0.5
Coulomb friction (N)	c_0	15
Friction difference (N)	c_s	10
Stribeck velocity coefficient (sm^{-1})	α	1
Sliding length (m)	D_0	0.002
Surface contact area coefficient	a	0.1

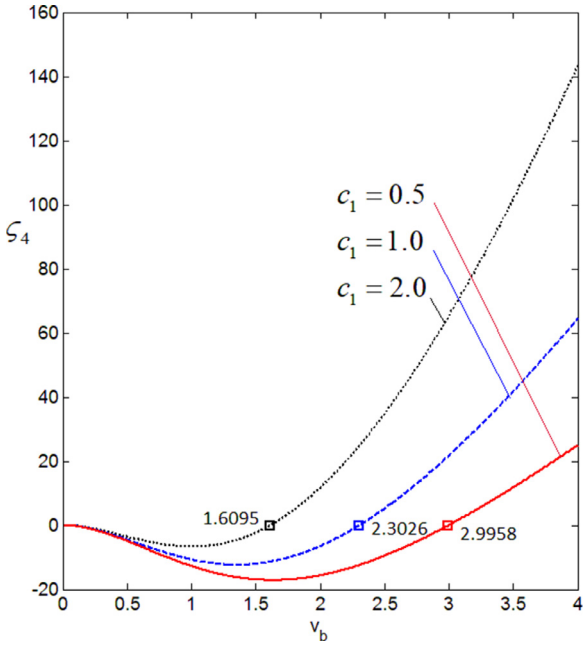

Fig. 3. Plots of curve $\varsigma_4 = \varsigma_4(v_b)$ with various values of viscous damping coefficient c_1 for determining velocity range of belt corresponding to stable state of equilibrium point. The zero-points 2.9958, 2.3026, 1.6095 in the graphs of the curve ς_4 are corresponding to the cases $c_1 = 0.5, 1.0, 2.0$.

Table 2
Values of zero-points of function $\varsigma_4(v_b)$ with various values of viscous damping coefficients c_1 for two models: LuGre and present two-state friction models.

c_1	0.2	0.3	0.5	1.0	1.5	2.0	2.5	3.0	3.5	4.0
LuGre	3.9120	3.5066	2.9957	2.3026	1.8971	1.6094	1.3863	1.2039	1.0498	0.9162
Present	3.9121	3.5066	2.9958	2.3026	1.8972	1.6095	1.3864	1.2040	1.0499	0.9164

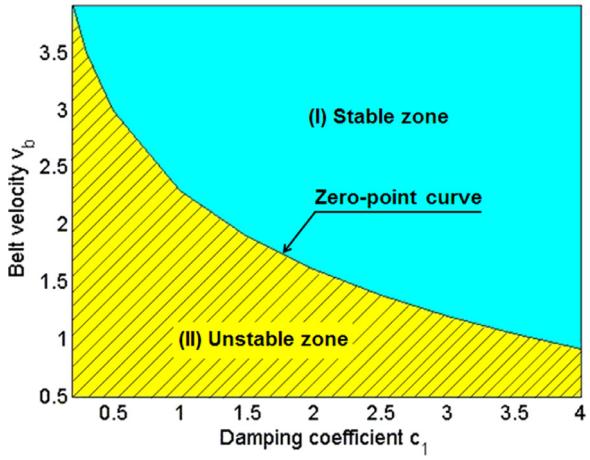

Fig. 4. Plot of zero-point curve of the function $\varsigma_4(v_b)$ versus the viscous damping coefficient c_1. The stable zone (I) and unstable zone (II) are separated by the zero-point curve, called boundary velocity curve.

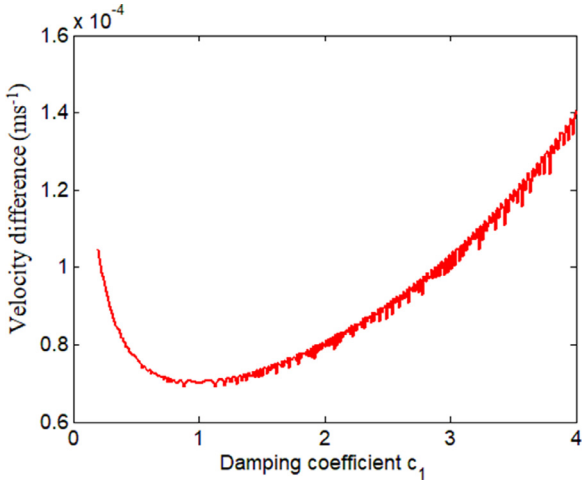

Fig. 5. Difference between values of zero-point curves corresponding to the present friction model and LuGre model. Zero-points corresponding to the LuGre model are obtained by solving the last equation of Eqs. (34), i.e. $\tilde{I}_1\tilde{I}_2 - \tilde{I}_0 = 0$.

method for Eq. $\varsigma_4(v_b) = 0$. The equilibrium point is stable if the belt velocity v_b is on the range $v_b > v_{b,ZP}$. In the following, the value $v_{b,ZP}$ is called the *boundary velocity*. In Fig. 3, for $c_1 = 0.5\ (\mathrm{Nsm}^{-1})$, the point $v_{b,ZP}$ is found to be $v_{b,ZP} = 2.9958\ (\mathrm{ms}^{-1})$. For larger viscous damping value $c_1 = 2.0\ (\mathrm{Nsm}^{-1})$, value of zero-point $v_{b,ZP}$ is shifted to left, i.e. $v_{b,ZP} = 1.6095\ (\mathrm{ms}^{-1})$. Table 2 presents calculation data of finding zero-points $v_{b,ZP}$ with ten different values of viscous damping coefficient c_1 for two cases: the present and LuGre models. The zero-points corresponding to the LuGre model are obtained from Eq. $\tilde{I}_1\tilde{I}_2 - \tilde{I}_0 = 0$ [see (34)]. It is observed that the zero-points obtained from the LuGre model are smaller than those obtained from the present two-state model. This reveals that dwell-time effect makes friction force larger, and therefore the belt needs a corresponding larger speed value to keep the mass block at equilibrium point.

Fig. 4 displays the graph of data in Table 2 for the present two-state model. The curve of zero-point $v_{b,ZP}$ versus the damping coefficient c_1 illustrates a boundary of stable zone (I) and unstable zone (II) for present model with dwell-time effect. The increase of viscous damping leads to a result in which the boundary velocity $v_{b,ZP}$ will be pulled down to a lower level. That means the stable state can be reached at low velocity and large damping. The difference between zero-points of two models is demonstrated in Fig. 5 via the numerical simulation with a set value of damping coefficient c_1 varying from 0.2 to 4.0 (Nsm^{-1}). The smallest difference value is reached at about $c_1 = 1\ (\mathrm{Nsm}^{-1})$ whereas the evident difference is at large value of viscous damping. The positive difference exhibits that the presence of the dwell-time effect has caused a small shift of stable zone to the direction of increase of belt velocity in comparison with stable zone obtained from the LuGre model. The effect is evident at large value of viscous damping because the factor of increasing damping makes motion of mass block become slower.

The stable and unstable zones of equilibrium point are also formulated in the plane $k - v_b$ for our present friction model. The numerical results for boundary velocity versus the spring stiffness k are depicted in Fig. 6. These results are obtained by solving Eq. $\varsigma_4(v_b) = 0$ with fixed value $c_1 = 0.5\ (\mathrm{Nsm}^{-1})$ and various values of stiffness k from

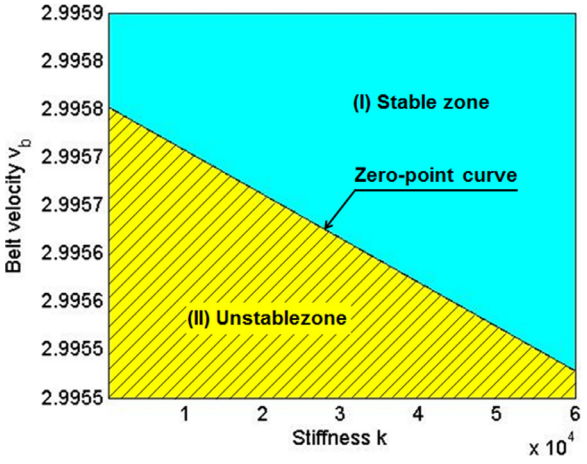

Fig. 6. Stable and unstable zones in plane $k - v_b$ for the present friction model are separated by the zero-point curve of the function $\varsigma_4(v_b)$ versus the stiffness parameter k. The value of k is taken from 100 to 60,000 Nm^{-1}.

100 to 60,000 (Nm^{-1}). The remaining used parameters are the same as in Fig. 4 (see Table 1). It is seen that the change of the boundary velocity versus the stiffness parameter k almost decreases linearly. In the considered range, $100 \le k \le 60000$, the increase of stiffness leads to the descent of belt velocity to attain the stable state of equilibrium point. This descent, however, is quite small, about $0.2 \times 10^{-3}\ (\mathrm{ms}^{-1})$ from the maximum to minimum values of boundary velocity curve. Fig. 7 shows that the difference of values of zero-point curves between the present and LuGre models in plane $k - v_b$ is positive in the considered range of belt velocity. There is a slight shift of zero-point curve of the present model in the direction of increase in belt velocity in comparison with that of the LuGre model. This mechanism reveals the effect of dwell-time, i.e. it can make the motion of mass element become heavier due

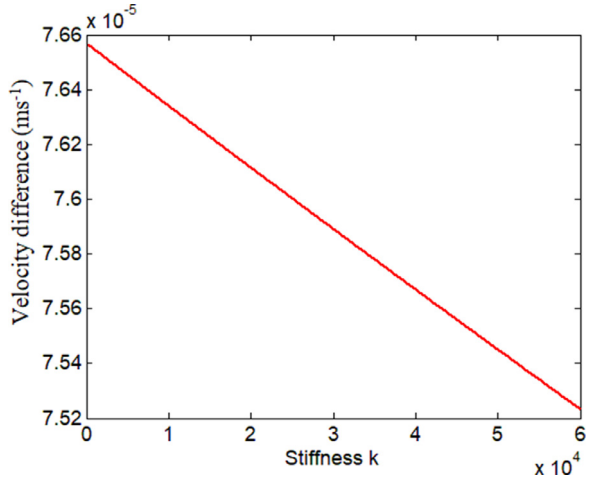

Fig. 7. Difference between values of zero-point curves corresponding to the present friction model and LuGre model in plane $k - v_b$.

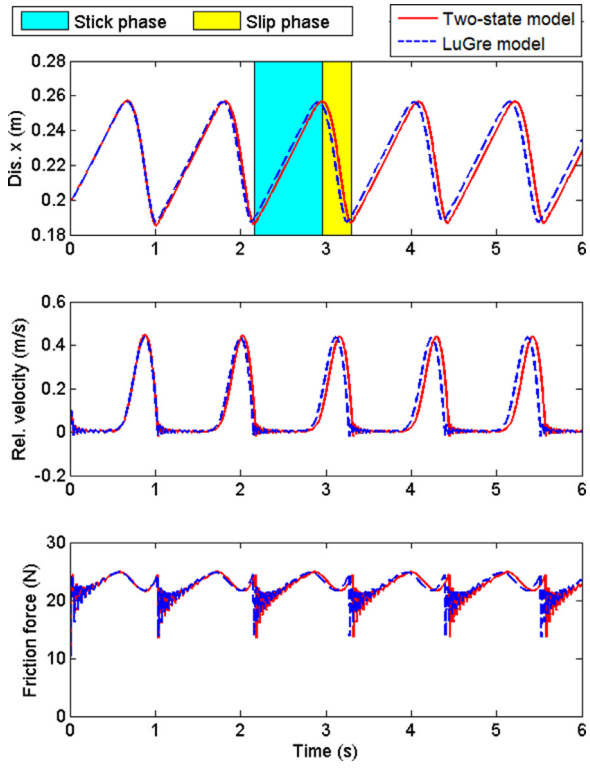

Fig. 8. Plots of evolutions of displacement x, relative velocity $v_{re} = v_b - \dot{x}$ and friction force for the two-state and LuGre models in case of belt velocity $v_b = 0.1$. The time intervals of stick and slip phases are distinguished by cyan and yellow colors (color online). (For interpretation of the references to colour in this figure legend, the reader is referred to the web version of this article.)

to the increasing friction effect, and a larger belt velocity is needed to keep the mass at the equilibrium point.

4.2. Stick-slip motion analysis with two friction models

In this subsection, we investigate the behavior of stick-slip motion of mass block on the belt for the two-state and LuGre models. Parameters in our simulation for Eqs. (8 a,b,c) are given in Table 1. Numerical results are shown in Figs. 8–15.

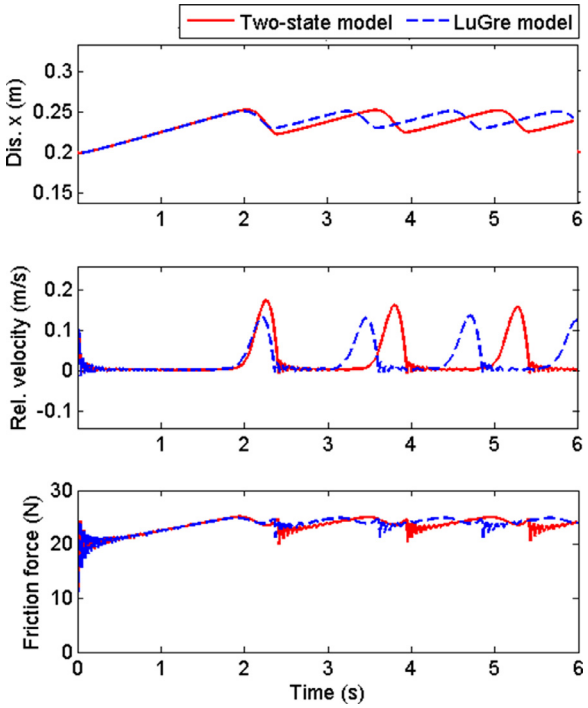

Fig. 9. Comparison of evolutions of displacement x, relative velocity $v_{re} = v_b - \dot{x}$ and friction force for the two-state and LuGre models in case of small belt velocity $v_b = 0.03$. The initial condition is chosen to be $[0.2\ 0.1\ 0\ 0]^T$ for displacement, velocity, internal variable z and dwell-time ϕ, respectively.

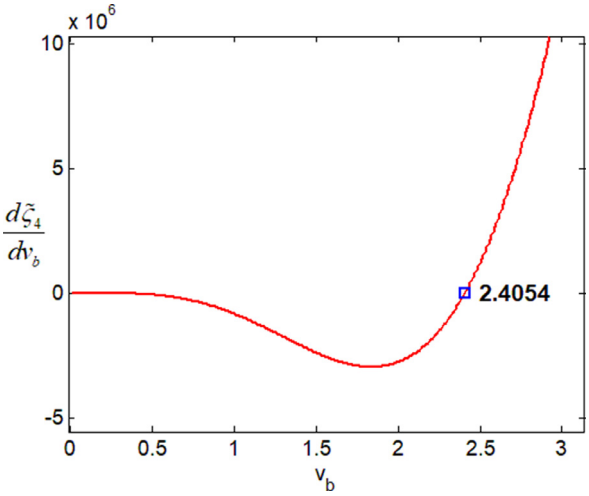

Fig. 10. Graph of $d\xi_4/dv_b$ and its zero-point.

In Fig. 8, results for displacement $x(t)$, relative velocity $v_{re} = v_b - \dot{x}$ and friction force F_{fr} corresponding to two models are compared in time domain. The time interval is taken to be [0, 6] (s). The initial condition $\begin{bmatrix} x(0) & \dot{x}(0) & z(0) & \phi(0) \end{bmatrix}^T$ in our simulation for the system state vector is chosen to be $\begin{bmatrix} 0.2 & v_b & 0 & 0 \end{bmatrix}^T$, where $\dot{x}(0) = v_b = 0.1$ guarantees that at the initial relative velocity, there is no deformation of bristle and initial deflection $z(0)$ is set to be zero. The dwell-time variable is of zero and the mass block is at rest on the belt at the starting time of motion. The expression for friction force is determined from Eq. (6) where the notation v is replaced by relative velocity $v_b - \dot{x}$. This expression occurs in the right-hand side of Eq. (8a). The initial value of friction force determined from the initial condition of system state is zero.

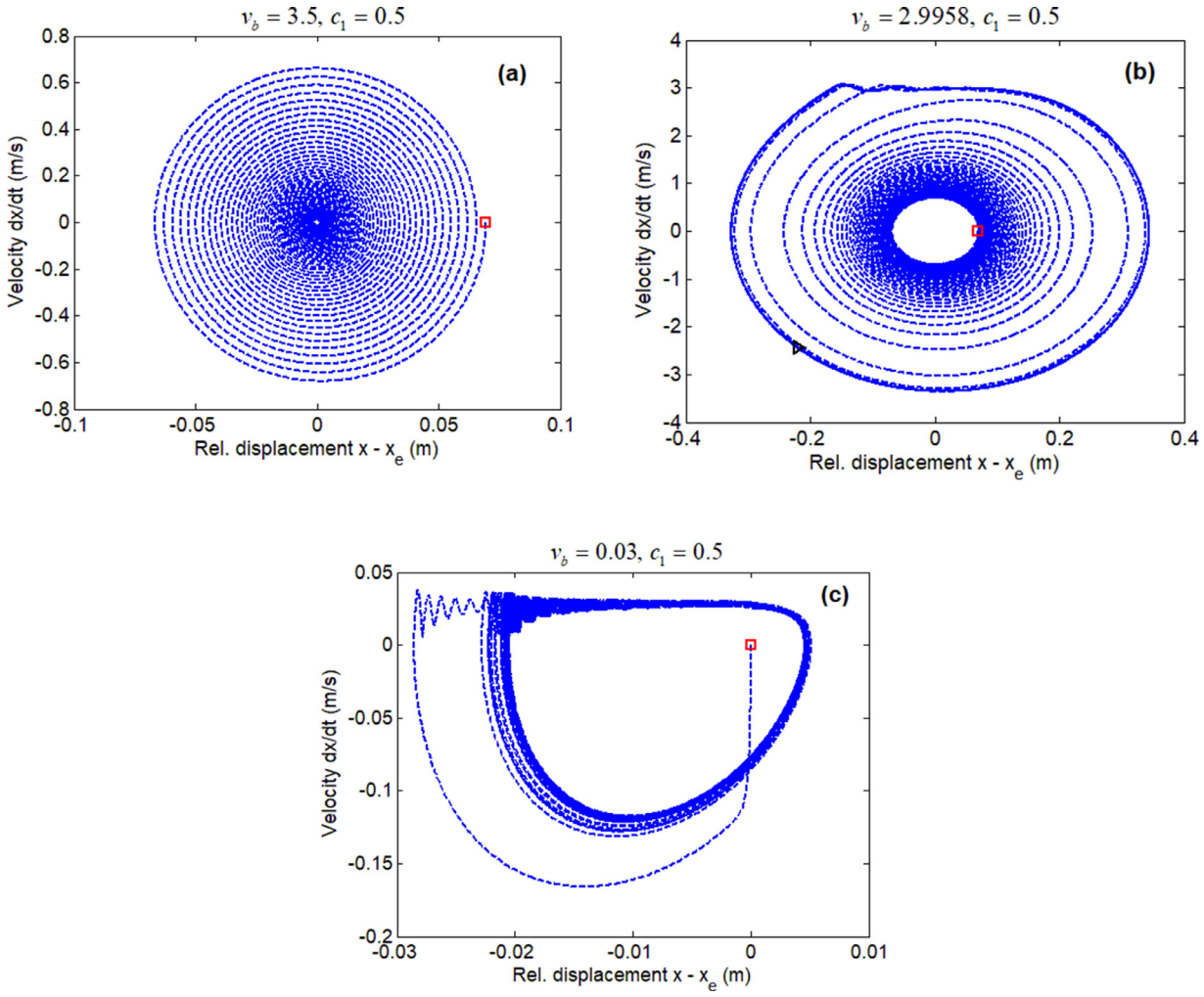

Fig. 11. The phase trajectories of $x - x_e$ and $\dot{x}$ for three cases of point (c_1, v_b): $S_1(0.5, 3.5), S_2(0.5, 2.9958), S_3(0.5, 0.03)$ belong to stable zone, boundary curve and unstable zone. Squared shape notation: starting point of phase trajectory.

In the first interval of time, about 0.6 (s), the mass block is in stick phase in which it is kept on the belt with near-zero relative velocity. This is because the friction force is predominant, the spring force is not enough large to overcome the magnitude of this friction force. Due to the existence of micro-motion during stick phase, the relative velocity between surfaces of belt and mass block is different from zero with very small relative value. This leads to the variation of friction force from zero at rest to non-zero values during motion because the micro-motion is related to the time-varying of internal state variable response of bristle in the friction model. [*The internal variable was introduced in the LuGre model to capture the micro-motions that affects the change of friction force during stick phase*].

When spring force is larger than friction force, the mass block starts moving on the belt and the stick phase is replaced by a slip phase. During slip motion, relative velocity is increasing considerably in time in comparison with that of stick phase. After a maximum value of relative velocity v_{re} is reached, this velocity begins to decrease gradually to near-zero values. There is a phenomenon of rapidly dropping of friction force at near-zero relative velocity before increasing again to compensate for the force from spring.

It is observed from Fig. 8 that the system motion is almost periodic with two phases of stick and slip changing alternatively. The system behaviors obtained from two models have similar shapes. However, due to the consideration of dwell-time effect, the system behavior of the two-state model has a delay in phase in comparison with that of the LuGre model. This is because the dwell-time effect between two surfaces makes them keep in contact in a longer time. This is observed and confirmed from experiment by Simoni et al. [28] for a joint mechanism of industrial robot manipulator.

The phase delay interval will expand if relative velocity v_{re} has smaller values, for example, $v_b = 0.03$ in Fig. 9. The effect of dwell-time is obvious in the case of small velocity of belt. This observation suggests that, for slow motion of mass block on the belt, one may prefer to use the model of two internal state variables to attain the higher precision in calculating motion trajectory of the system, especially in the problem of precise control. There is a small difference of friction force between two models because of the presence of the Simoni's added area term $s_t = a\left(1 - \exp\left\{-\phi/\phi_0\right\}\right)$ in expression of friction force of the present two-state model. The effect of this term is larger if dwell-time increases.

4.3. Formulation of limit cycle via Hopf bifurcation

Analytical expressions for occurence conditions of Hopf bifurcation are given in (37) and (38). We now check these conditions via numerical evaluations with given parameters of the system. The condition $\tilde{\varsigma}_4 = \tilde{b}_1\tilde{b}_2\tilde{b}_3 - \tilde{b}_0\tilde{b}_3^2 - \tilde{b}_1^2 = 0$ in (37) gives the equation of determining restrained curves of parameters at which the stability of the equilibrium point $\mathbf{w}_e$ changes as one of system parameters varies. We focus on the bifurcation parameter v_b to show the effect of belt velocity on system's motion, especially in the regime of low velocity motion. For the condi-

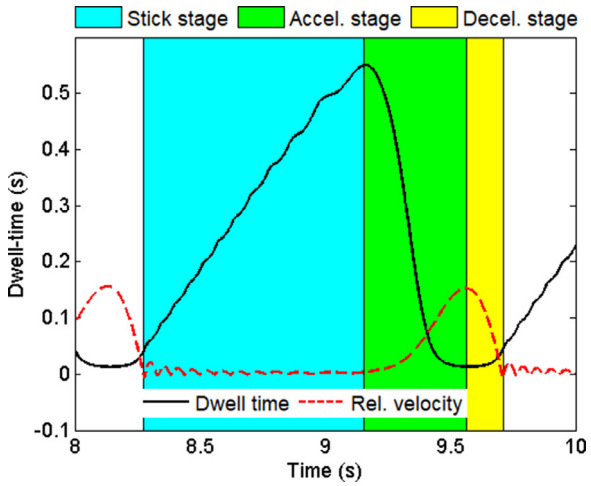

Fig. 12. Evolutions of dwell-time and relative velocity in the time interval [8, 10] (s) for case $v_b = 0.03$ [cyan color: stick stage; green color: acceleration stage; yellow color: deceleration stage]. (For interpretation of the references to colour in this figure legend, the reader is referred to the web version of this article.)

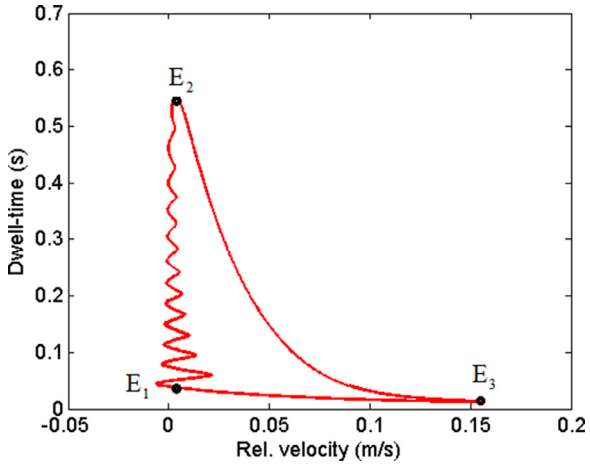

Fig. 13. Dwell-time as a function of relative velocity for case $v_b = 0.03$. The limit cycle for relationship of dwell-time and relative velocity can be divided into three main stages of cycle: near-zero velocity stage E_1E_2, acceleration stage E_2E_3 and deceleration stage E_3E_1.

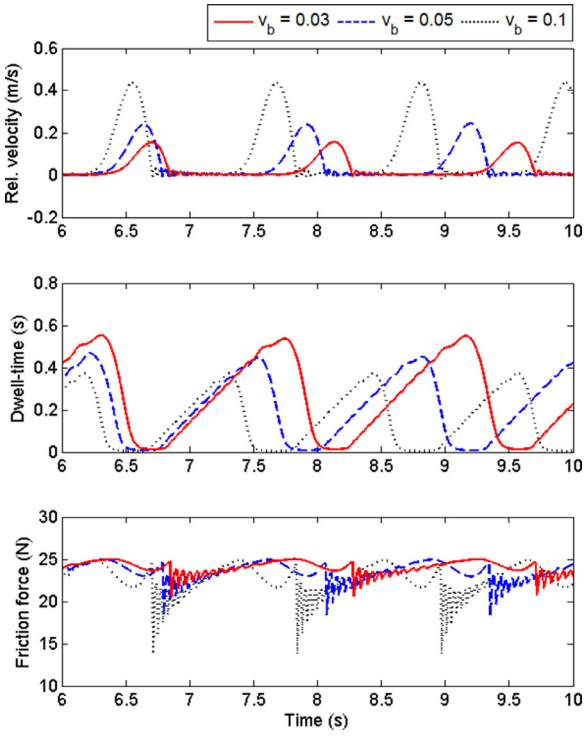

Fig. 14. Plots of the change of relative velocity, dwell-time and friction with three different values of belt velocity: $v_b = 0.03,\ 0.05,\ 0.1$.

tion (38), the graph of curve $d\tilde{\varsigma}_4/dv_b$ for $c_1 = 0.5$ is ploted in Fig. 10. The zero-point of $d\tilde{\varsigma}_4/dv_b$ for $c_1 = 0.5$ is found to be 2.4054 that is marked by a squared shape in Fig. 10.

In Fig. 4, we select two different points, a point $S_1(c_1, v_b) = (0.5, 3.5)$ lies on the stable zone (I) and a point $S_3(c_1, v_b) = (0.5, 0.03)$ belongs to the unstable zone (II). The selection of v_b should be different from $v_b = 2.4054$ that is solution of $d\tilde{\varsigma}_4/dv_b$. For the first case, S_1, in the phase plane $(x - x_e, \dot{x})$, the starting point for motion trajectory is at $(0.0695, 0)$, i.e. we choose initial condition $[x(0), \dot{x}(0), z(0), \phi(0)] = [0.24, 0, 0, 0]$ for our simulation. For the second case S_3, we choose $[x(0), \dot{x}(0), z(0), \phi(0)] = [x_e, 0, 0, 0]$ where x_e is determined from Eq. (11). The phase trajectories for two cases S_1 and S_3 are ploted in Fig. 11a,c. Fig. 11a shows that the equilibrium point $\mathbf{w}_e$ is stable. After a long time, the displacement $x(t)$ approaches to the equilibrium value x_e whereas the velocity $\dot{x}$ tends to zero. That means the mass block is almost motionless in x-coordinate although the belt is still moving with velocity v_b. The velocity $v_b = 3.5$ is considered as a large value in comparison with the velocity $v_b = 0.03$ in the regime of low velocity motion. At $v_b = 0.03$, the phase trajectory portrayed in Fig. 11c exhibits a limit cycle after a long time of motion. It is seen that the equilibrium point $\mathbf{w}_e$ is unstable in the range of low velocity that is smaller than zero-point. In our situation, the zero-point is found to be $v_{b,ZP} = 2.9958$. In Fig. 4, at boundary point S_2 with $v_{b,ZP} = 2.9958$ and $c_1 = 0.5$, the phase trajectory is shown in Fig. 11b with initial condition $[x(0), \dot{x}(0), z(0), \phi(0)] = [0.24, 0, 0, 0]$. This trajectory is approaching to a limit cycle as time tends to infinity. From the behaviors of phase trajectories in Fig. 11, we can say that the system has undergone a supercritical Hopf bifurcation. The exploration of effects of two parameters k and c_1 on the behavior of Hopf bifurcation is done in the same way.

4.4. Influence of belt velocity on phases of stick-slip motion

To explore the effect of belt velocity v_b on the relative velocity, dwell-time and friction force responses, we select three cases $v_b = 0.03, 0.05, 0.1$ for our simulation. The obtained results are illustrated in Figs. 12–14 in time interval [6, 10] (s) in which the steady-state of responses can be attained. For the first case $v_b = 0.03$, relative velocity is quite small. This slow motion will make surfaces be kept in contact in a longer time. Consequently, the dwell-time response increases in stick phase. Fig. 12 shows that the behavior of dwell-time is nearly linear in stick phase, for example, in time interval [8.25, 9.15] (s). It can be shown that the dwell-time is always positive for all time. In the slip phase, however, the dwell-time has very small positive value. The dwell-time will disappear if the system is in the grossing slip state and has not stick motion. The dependence of dwell-time on relative velocity is portrayed in Fig. 13 for the case $v_b = 0.03$. It is seen that at steady-state regime of stick-slip motion, a limit cycle can be formulated. The limit cycle for relationship of dwell-time and relative velocity can be divided into three main stages of cycle: (I) near-zero velocity stage, (II) acceleration stage and (III) deceleration stage. The stage (I) is corresponding to the stick phase of motion, illustrated on a curve segment E_1E_2 in Fig. 13. In this stage, there is a slight oscillation phenomenon of dwell-time about zero-relative velocity. The stage (II), depicted in curve segment E_2E_3, is corresponding to the growing state of relative velocity v_{re} in slip phase because in this stage, the spring force is enough large to win the friction force and causes a sliding motion of mass block. The stage (III) displayed

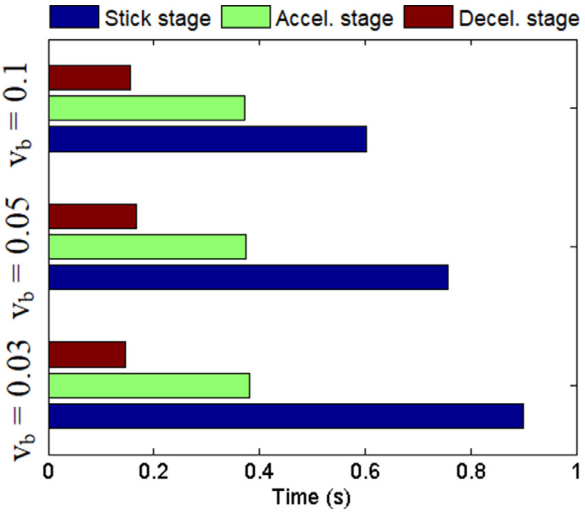

Fig. 15. Duration of stick stage (I), acceleration stage (II), and deceleration stage (III) in three cases of belt velocity $v_b = 0.03,\ 0.05,\ 0.1$. The duration of stick phase is increasing with decreasing of belt velocity.

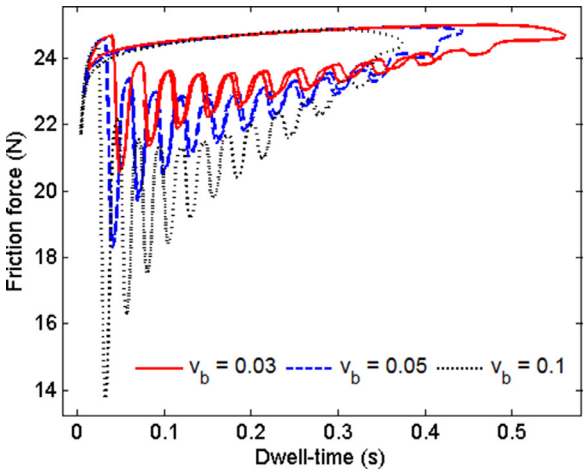

Fig. 16. Friction force as a function of dwell-time in the cases $v_b = 0.03, 0.05, 0.1$. For the stick phase, the friction force in the case of low belt velocity $v_b = 0.03$ is higher than remaining cases with higher belt velocity.

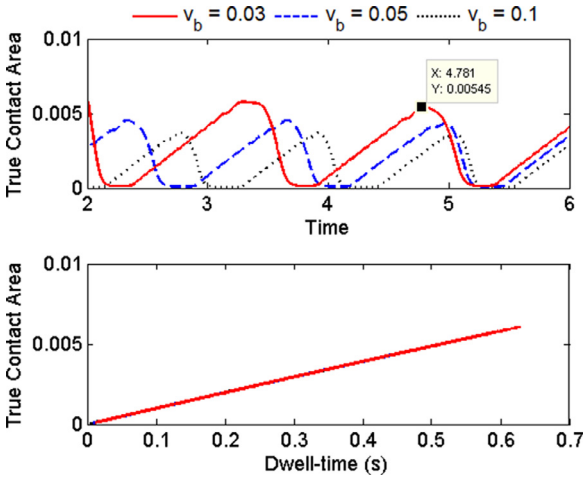

Fig. 17. Plots of the change of true contact area in time and in dwell-time. The true contact area will expand if the belt velocity decreases from 0.1 to 0.03 (ms^{-1}).

on the curve segment E_3E_1 is the stage of reducing of relative velocity and mass block motion has a tendency to end a period of stick-slip vibration. The formation of two stages (II) and (III) in Fig. 13 shows the change of the process of transferring energy between spring and friction forces. In stage (II), the energy of spring force is compensated by the loss part of the friction energy whereas in the stage (III) the trend of energy equilibrium state is established from the increase of friction force due to the effect of dwell-time. The dwell-time value of stage (II) is larger than that of stage (III).

Fig. 14 shows the influence of the belt velocity on the behavior of relative velocity, dwell-time and friction force in three cases $v_b = 0.03, 0.05, 0.1$. If increasing the velocity v_b, the peak of relative velocity is uplifted and has a shift to the left. In these simulated cases, the case $v_b = 0.03$ gives system's motion with slowest relative velocity but the longest time of stick phase. Against, the largest relative velocity and shortest time of stick phase belong to the case $v_b = 0.1$. The estimated durations of stick stage (I), acceleration stage (II), and deceleration stage (III), respectively, are about 0.9, 0.38, 0.15 (s) for the case $v_b = 0.03$ and 0.60, 0.37, 0.156 (s) for the case $v_b = 0.1$. The data of simulation are illustrated by bars in Fig. 15. It is seen that the duration of stick phase is increasing with decreasing of belt velocity. In the slip phase, however, the change of duration of stages (II) and (III) is not considerable.

The dependence of friction force on the dwell-time is illustrated in Fig. 16 for cases $v_b = 0.03,\ 0.05,\ 0.1$. In Figs. 14 and 16, for the stick phase, the friction force in the case of low belt velocity $v_b = 0.03$ is higher than remaining cases with higher belt velocity.

Fig. 17 demonstrates the change of true contact area $s_t = a(1 - \exp\{-\phi/\phi_0\})$ in time and in dwell-time. The true contact area will expand if the belt velocity decreases from 0.1 to 0.03 (ms^{-1}). The dependence of the true contact area on dwell-time is nearly linear because for small dwell-time value, we have an approximation $s_t = a\phi/\phi_0$.

5. Conclusions and remarks

The new point of present research is to introduce a two-state model, recently developed by Simoni et al. to study the problem of motion of a spring-mass system placed on a belt moving at constant low speed. The low velocity of the belt is considered in our study because at this velocity, the influence of two internal state variables is evident. The first state variable was included in the LuGre model to capture the Stribeck effect in motions with the relatively low velocity between two surfaces. The second state variable proposed by Simoni et al. is based on a combination of the LuGre model and Dieterich-Ruina model to capture the dwell-time effect of motion between two surfaces in which the friction force increases if two surfaces are kept in contact in a certain time. Two internal state variables included in the model are considered as a more realistic description than the LuGre model with only one internal state variable. Calculations for our model, however, will be more complicated than those for the LuGre model because the total number of state variables of the system is four (two conventional state variables are displacement and velocity; and two internal state variables are bristle deflection and dwell-time) whereas that of the system using the LuGre model is three (without dwell-time variable). The research results are shown in the following main points:

- The equilibrium point position of the system is investigated in the friction-induced vibration model with the presence of the dwell-time effect. We obtain an analytical expression of an added equilibrium displacement generated by the dwell-time effect. If considering this added displacement as a function of belt velocity, the result shows that it is a monotonically decreasing function and is bounded in a specified interval.
- Stable property of the equilibrium point of the system is examined using the Routh-Hurwitz criterion for a quartic characteristic equation of the matrix corresponding to the linearized system of the orig-

inal nonlinear system around the equilibrium position. The calculation results have exhibited two zones of stability and instability with common boundary being a curve containing zero-points of an equation obtained from Routh-Hurwitz criterion. Because of the presence of dwell-time effect, we show that there is a small shift of the stable zone in the increasing direction of belt velocity relative to the stable zone obtained from the LuGre model.
- The formulation of limit cycle in the regime of low velocity motion is presented via Hopf bifurcation analysis.
- Analysis of stick-slip motion using the two-state model shows the effect of dwell-time in the case of small belt velocity, i.e. the effect of increasing friction force with slow motion of the belt (the LuGre model does not capture this effect).
- Three stages of the stick-slip motion are analyzed in detail, which show that the time duration of dwell-time phase is significant in the case of the low relative velocity between the mass block and belt surfaces. The stick-slip vibration generates limit cycles of system motion, in which the limit cycle in plane of the relative velocity - dwell-time is presented.

Experimental study of frictional systems is a complex problem, especially for models that consider many different effects. Our research problem is based on the two-state model recently proposed by Simoni. The Simoni's model was experimentally verified on an industrial robotic arm to evaluate the influence of dwell-time on torque response of robot joints at low velocity motion regime. In our opinion, this is a potential model for further studies of complex systems in both analytical and numerical approaches. Based on the empirical evidence of the Simoni's model, it motivates us to study the stick - slip motion of system models in engineering that takes into account the dwell-time effect using approach of theoretically qualitative analysis combined with numerical analysis. Therefore, the results of the paper initially provide theoretical insights for the system under consideration. The experimental result for confirming the behavior of the system is necessary and should be studied in the future.

Declaration of Competing Interest

We know of no conflict of interest associated with this publication. As corresponding author, I confirm that the manuscript has been read and approved for submission by all the named authors.

CRediT authorship contribution statement

N.N. Hieu: Conceptualization, Methodology, Investigation, Writing - review & editing. **P.N. Chung:** Investigation, Writing - original draft, Writing - review & editing.

Acknowledgment

The first author was supported by Vietnam Academy of Science and Technology (VAST) (code: VAST01.03/18-19). The second author was supported by grant with code T19-26 from the University of Mining and Geology.

References

[1] Brian AH. Control of machines with friction. New York: Springer Science + Bussiness Media; 1991.
[2] Guran A, Pfeiffer F, Popp K. Dynamics with friction: modeling, analysis and experiment. World Scientific Publishing; 2001.
[3] Wiercigroch M, Kraker B. Applied nonlinear dynamics and chaos of mechanical systems with discontinuities. World Scientific 2000. doi:10.1142/3345.
[4] Saha A, Wiercigroch M, Jankowski K, Wahi P, Stefanski A. Investigation of two different friction models from the perspective of friction-induced vibrations. Tribol Int 2015;90:185–97.
[5] Wang DW, Mo JL, Zhang Q, Zhao J, Ouyang H, Zhou ZR. The effect of the grooved elastic damping component in reducing friction-induced vibration. Tribol Int 2017;110:264–77. doi:10.1016/j.triboint.2017.02.031.
[6] Liu N, Ouyang H. Friction-induced vibration of a slider on an elastic disc spinning at variable speeds. Nonlinear Dyn 2019;98:39–60.
[7] Dupont PE. Avoiding stick-slip in position and force control through feedback. Advanced Practical Process Control. Berlin Heidelberg: Springer-Verlag; 2004.
[8] Oetstreich M, Hinrichs N, Kopp K. Bifurcation and stability analysis for a non-smooth friction oscillator. Archive Applied Mechanics 1996;66:301–14.
[9] Pratt TK, Williams R. Non-linear analysis of stick/slip motion. J Sound Vib 1981;74:531–42.
[10] Thomsen JJ, Fidlin A. Analytical approximations for stick-slip vibration amplitudes. Int J Non Linear Mech 2003;38:389–403.
[11] Khulief YA, Al-Sulaiman FA, Bashmal S. Vibration analysis of drillstrings with self-excited stick-slip oscillations. J Sound Vib 2007;299:540–58.
[12] Sinou JJ, Dereure O, Mazet GB, Thouverez F, Jezequel L. Friction-induced vibration for an aircraft brake system-part 1: experimental approach and stability analysis. Int J Mech Sci 2006;48:536–54. https://www.springer.com/gp/book/9780792391333
[13] Armstrong-Hélouvry B, Dupont P, Canudas de Wit C. A survey of models, analysis tools and compensation methods for the control of machines with friction. Automatica 1994;30:1083–138. doi:10.1016/0005-1098(94)90209-7.
[14] Olsson H, Åström KJ, Canudas de Wit C, Gäfvert M, Lischinsky P. Friction models and friction compensation. European Journal of Control 1998:176–95. doi:10.1016/S0947-3580(98)70113-X.
[15] Awrejcewicz J, Olejnik P. Analysis of dynamic systems with various friction laws. Appl Mech Rev 2005;58:389–411.
[16] Mostaghel N, Davis T. Representations of coulomb friction for dynamic analysis. Earthquake Engineering & Structural Dynamics 1997;26:541–8. https://onlinelibrary.wiley.com/doi/abs/10.1002/(SICI)1096-9845(199705)26:5%3C541::AID-EQE6603E3.0.CO;2-W.
[17] Niranjan P, Karinka S, Sairam K. Friction modeling in servo machines: a review. International Journal of Dynamics and Control 2017;6:893–906.
[18] Liang JW, Feeny BF. Identifying coulomb and viscous friction from free-vibration decrements. Nonlinear Dyn 1998;16:337–47. doi:10.1023/A:1008213814102.
[19] Dahl PR. A solid friction model. Tech. rep.. Los Angeles, CA (USA): Space and Missile Systems Organization, Air Force System Command; 1968. ADA041920
[20] Stribeck R. Die wesentlichen eigenschaften der gleit- und rollenlager - the key qualities of sliding and roller bearings. Z Ver Dtsch Ing 1902;46:38–9.
[21] Bliman PA. Friction modelling by hysteresis operators : application to dahl, sticktion and stribeck effects. In: Proc. Conf. on Models of Hysteresis, Trento; 1991.
[22] Canudas de Wit C, Olsson H, Åström KJ, Lischinsky P. A new model for control of systems with friction. IEEE Trans Automat Contr 1995;40:419–25.
[23] Canudas de Wit C. Comments on "a new model for control of systems with friction". IEEE Trans Automat Contr 1998;43:1189–90.
[24] Barabanov R, Ortega N. Necessary and sufficient conditions for passivity of the lugre friction model. IEEE Trans Automat Contr 2000;45:830–2.
[25] Altpeter F. Friction modeling, identification and compensation. Ecole Politechnique Federal de Lausanne; 1999. Ph.d. dissertation. [Online]. Available: http://library.epfl.ch/theses/?nr=1988
[26] Berger EJ. Friction modeling for dynamic system simulation. Appl Mech Rev 2002;55:535–77.
[27] Do NB, Ferri AA, Bauchau OA. Efficient simulation of a dynamic system with lugre friction. J Comput Nonlinear Dyn 2007;2:281–9.
[28] Wojewoda J, Stefanski A, Wiercigroch M, Kapitaniak T. Hysteretic effects of dry friction modelling and experimental studies. Philosophical Transactions Mathematical Physical & Engineering Sciences 2008;366:747–65.
[29] Marques F, Flores P, Pimenta CJC, Lankarani HM. A survey and comparison of several friction force models for dynamic analysis of multibody mechanical systems. Nonlinear Dyn 2016;86:1407–43. doi:10.1007/s11071-016-2999-3.
[30] Marques F, Flores P, Claro JCP, Lankarani HM. Modeling and analysis of friction including rolling effects in multibody dynamics: a review. Multibody Syst Dyn 2018;45:223–44. doi:10.1007/s11044-018-09640-6.
[31] Al-Bender F, Lampaert V, Swevers J. A novel generic model at asperity level for dry friction force dynamics. Tribol Lett 2004;16:81–93. doi:10.1023/b:tril.0000009718.60501.74.
[32] Dupont P, Armstrong B, Hayward V. Elasto-plastic friction model: contact compliance and stiction. In: Proceedings of the 2000 American Control Conference. ACC (IEEE Cat. No.00CH36334); 2000. p. 1072–7.
[33] Ettore P, Valerio R, Pietro S, Paolo VP. Review and comparison of dry friction force models. Nonlinear Dyn 2016;83:1785–801.
[34] Gonthier Y, McPhee J, Lange C, Piedbœuf JC. A regularized contact model with asymmetric damping and dwell-time dependent friction. Multibody Syst Dyn 2004;11:209–33.
[35] Saha A, Wahi P, Wiercigroch M, Stefanski A. A modified lugre friction model for an accurate prediction of friction force in the pure sliding regime. Int J Non Linear Mech 2016;80:122–31. doi:10.1016/j.ijnonlinmec.2015.08.013.
[36] Krasnik V, Schlattmann J. An extended lugre friction model incorporating frictional aging. PAMM Proc Appl Math Mech 2016;16:283–4. doi:10.1002/pamm.201610130.
[37] Pikunov D, Stefanski A. Numerical analysis of the friction-induced oscillator of duffing's type with modified lugre friction model. J Sound Vib 2019;440:23–33. doi:10.1016/j.jsv.2018.10.003.
[38] Canudas de Wit C, Kelly R. Passivity analysis of a motion control for robot manipulators with dynamic friction. Asian J Control 2007;9:30–6. doi:10.1111/j.1934-6093.2007.tb00301.x.
[39] Bittencourt AC, Wernholt E, Sander-Tavallaey S, Brogårdh T. An extended friction model to capture load and temperature effects in robot joints. In: IEEE/RSJ International Conference on Intelligent Robots and Systems (IROS); 2010. p. 6161–7. doi:10.1109/iros.2010.5650358.

[40] Bittencourt AC, Gunnarsson S. Static friction in a robot joint: modeling and identification of load and temperature effects. Journal of Dynamic Systems Measurement and Control 2012;134:051013. (10 pages)
[41] Yue F, Li X, Chen C, Tan W. Adaptive integral backstepping sliding mode control for opto-electronic tracking system based on modified lugre friction model. Int J Syst Sci 2017;48:3374–81. doi:10.1080/00207721.2017.1387315.
[42] Yue F, Li X. Robust adaptive integral backstepping control for opto-electronic tracking system based on modified lugre friction model. ISA Trans 2018;80:312–21. doi:10.1016/j.isatra.2018.07.016.
[43] Wang H, Leaney PG. A new friction model in hybrid pump-controlled asymmetric (single-rod) cylinder drive system. Tribol Trans 2020. doi:10.1080/10402004.2020.1762955.
[44] Yanada H, Sekikawa Y. Modeling of dynamic behaviors of friction. Mechatronics 2008;18:330–9.
[45] Tran XB, Hafizah N, Yanada H. Modeling of dynamic friction behaviors of hydraulic cylinders. Mechatronics 2012;22:65–75.
[46] Deur J, Ivanovic V, Troulis M, Miano C, Hrovat D, Asgari J. Extensions of the lugre tyre friction model related to variable slip speed along the contact patch length. Veh Syst Dyn 2005:508–24. doi:10.1080/00423110500229808.
[47] Yongjie L, Junning Z, Shaopu Y, Zhenyu L. Study on improvement of lugre dynamical model and its application in vehicle handling dynamics. J Mech Sci Technol 2019;33:545–58. doi:10.1007/s12206-019-0108-5.
[48] Sobczyk MR, Perondi EA, Cunha MAB. A continuous extension of the lugre friction model with application to the control of a pneumatic servo positioner. In: IEEE Conference on Decision and Control (CDC); 2012. p. 3544–50. doi:10.1109/cdc.2012.6426406.
[49] Dankowicz H. On the modeling of dynamic friction phenomena. ZAMM - Journal of Applied Mathematics and Mechanics / Zeitschrift für Angewandte Mathematik und Mechanik 1999;79:399–409. doi:10.1002/(sici)1521-4001(199906)79:6<399::aid-zamm399>3.0.co;2-k.
[50] Al-Bender F, Lampaert V, Swevers J. Modeling of dry sliding friction dynamics: from heuristic models to physically motivated models and back. Chaos: An Interdisciplinary Journal of Nonlinear Science 2004;14:446. doi:10.1063/1.1741752.
[51] Dupont P, Hayward V, Armstrong B, Altpeter F. Single state elasto-plastic friction models. IEEETransAutomControl 2002;47:787–92.
[52] Ferretti G, Magnani G, Rocco P. Single and multistate integral friction models. IEEE Trans Automat Contr 2004;49:2292–7. doi:10.1109/TAC.2004.839234.
[53] Armstrong B, Chen Q. Thez-properties chart. IEEE Control Syst Mag 2008;28:79–89.
[54] Ruderman M, Bertram T. Two-state dynamic friction model with elasto-plasticity. Mech Syst Signal Process 2013;39:316–32.
[55] Berthoud P, Baumberger T, G'Sell C, Hiver JM. Physical analysis of the state- and rate-dependent friction law: static friction. Physical Review B 1999;59:14313–27.
[56] Baumberger T, Berthoud P, Caroli C. Physical analysis of the state- and rate-dependent friction law. ii. dynamic friction. Physical Review B 1999;60:3928–39.
[57] Baumberger T, Caroli C. Solid friction from stick-slip down to pinning and aging. Adv Phys 2006;55:279–384. doi:10.1080/00018730600732186.
[58] Gitis NV, Volpe L. Nature of static friction time dependence. J Phys D Appl Phys 1992;25(4):605.
[59] Heslot F, Baumberger T, Perrin B, Caroli B, Caroli C. Creep, stick-slip, and dry-fric- tion dynamics: experiments and a heuristic model. Physical Review E 1994;49(6):4973.
[60] Rice JR, Ruina AL. Stability of steady frictional slipping. J Appl Mech 1983;50(2):343–9.
[61] Simoni L, Beschi M, Visioli A, Åström KJ. Inclusion of the dwell time effect in the lugre friction model. Mechatronics 2020;66:102345.
[62] Dieterich JH. Modeling of rock friction: 1. experimental results and constitutive equations. J Geophys Res 1979;84(B5):2161–8.
[63] Routh EJ. A treatise on the stability of a given state of motion: particularly steady motion. Macmillan and Company; 1877.
[64] Hurwitz A. Ueber die bedingungen, unter welchen eine gleichung nur wurzeln mit negativen reellen theilen besitzt. Mathematische Annalen 1895;46:273–84. doi:10.1007/BF01446812.
[65] Rahman QI, Schmeisser G. Analytic theory of polynomials: critical points, zeros and extremal properties. USA: Oxford University Press; 2002.
[66] Anagnost JJ, Desoer CA. An elementary proof of the routh-hurwitz stability criterion. Circuits, Systems, and Signal Processing 1991;10:101–14.
[67] Hassard BD, Kazarinoff ND, Wan YH. Theory and applications of the hopf bifurcation. Cambridge: Cambridge University Press; 1980.
[68] Guckenheimer J, Holmes P. Nonlinear oscillations, dynamical systems, and bifurcations of vector fields-John guckenheimer. New York: Springer Science + Business Media; 1983.
[69] Leine RI, Nijmeijer H. Dynamics and bifurcations of non-Smooth mechanical systems. Berlin Heidelberg: Springer-Verlag; 2004.
[70] Liu WM. Criterion of hopf bifurcations without using eigenvalues. J Math Anal Appl 1994;182:250–6.